Hazard Assessment Comparison of Tazhiping Landslide Before and After Treatment using the Finite Volume Method

Dong Huang [1], YuanJun Jiang[1]*,JianPing Qiao[1], Meng Wang[1]

1. Key Laboratory of Mountain hazards and Surface process, Institute of Mountain hazards and Environment, Chinese Academy of Science, Chengdu 610041, China
*Corresponding author (yuanjun.jiang.civil@gmail.com).

Abstract: Through investigation and analysis of geological conditions and mechanical parameters of the Taziping landslide, the finite volume method was adopted, and, the rheological model was adopted to simulate the landslide and avalanche entire mass movement process. The present paper adopted the numerical approach of RAMMS and the GIS platform to simulate the mass movement process before and after treatment. This paper also provided the conditions and characteristic parameters of soil deposits (flow height, velocity, and stresses) during the landslide mass movement process and mapped the 3D division of hazard zones before and after landslide treatment. Results indicated that the scope of hazard zones contracted after engineering treatment of the landslide. The extent of high-hazard zones was reduced by about 2/3 of the area before treatment, and characteristic parameters of the mass movement process after treatment decreased to 1/3 of those before treatment. Despite engineering treatment, the Taziping landslide still poses significant hazard to nearby settlements. Therefore, we propose that houses located in high-hazard zones be relocated or reinforced for protection.

Keywords: finite volume method; rheological model; motion feature parameters; hazard assessment

1. Introduction

The hazards of a landslide include scope of influence (i.e., source area, possible path area, and backward and lateral expansion area) and secondary disasters (i.e., reservoir surge, blast, and landslide-induced barrier lake). A typical landslide hazard assessment aims to propose a systematic hazard assessment method with regard to a given position or a potential landslide. Current research on typical landslide hazard assessment remains immature, and there are multiple methods for interpreting landslide hazards. To be specific, the scope of influence prediction of a landslide refers to deformation and instability characteristics such as sliding distance, movement speed, and bulking thickness range. The movement behavior of a landslide mass is related to its occurrence, sliding mechanisms, mass characteristics, sliding path, and many other factors. Current landslide movement prediction methods include empirical prediction and numerical simulation.

Empirical prediction method: The empirical prediction method involves

analyzing landslide flow through the collection of landslide parameters in the field. It further consists of the geomorphologic method (Costa, 1984; Jackson et al., 1987; Scott et al., 1993), the geometric change method (Finlay et al., 1999; Michael-Leiba et al., 2003), and the volume change method (Fannin et al., 2001). Empirical models are commonly simple and easy to apply, and the required data are easy to obtain as well. **Numerical simulation method:** Numerical simulation methods are further divided into the continuous deformation analysis method (Hungr, 1995; Evans et al., 2009; Wang, et al., 2016), the discontinuous deformation analysis method (Shi, 1988), and the simplified analytical simulation method (Christen et al., 2010a; Sassa, 2010; Bartelt et al., 2012; Du et al., 2015). The numerical simulation method expresses continuous physical variables using the original spatial and temporal coordinates with geometric values of discrete points. Numerical simulations follow certain rules to establish an algebraic equation set in order to obtain approximate solutions for physical variables.

Empirical prediction models only provide a simple prediction of the sliding path. Due to the differences in geological environments, empirical prediction models commonly have low generality. The continuous deformation method has the advantage of an extremely strong replication capability, but it is not recommended when analyzing flow-type landslides, lahars, or debris flows because of complicated rheological behaviors (Iverson et al., 1997, 2001; Hungr et al., 2001; Glade 2005; Portilla et al., 2010; Chen et al., 2014). The fluid mechanics-based discontinuous deformation method has several shortcomings such as, great computational burden, difficult parameter selection, and difficult 3D implementation. The simplified analytical simulation method fully takes into account the flow state properties of landslides before introducing a rheological model and can easily realize 3D implementation on the GIS platform. On that account, this paper adopted the continuous fluid mechanics-based finite volume method (simplified analytical simulation method). We introduce a rheological model on the basis of using mass as well as momentum and energy conservation to describe the movement of landslides. We also employed GIS analysis to simulate the entire movement process of Taziping landslide and map the 2D division of hazard zones.

2. Methods

2.1 Kinetic analysis method

Adopting the continuous fluid mechanics-based finite volume method, this paper took into account erosion action on the lower surface of the sliding mass and the change in frictional resistance within the landslide-debris flow in order to establish a computational model. The basic idea is to divide the calculation area into a series of non-repetitive control volumes, ensuring that there is a control volume around each grid point. Each control volume is then integrated by the unresolved differential equation in order to obtain a set of discrete equations. The unknown variable is the numerical value of the dependent variable at each grid point. To solve the integral of a control volume, we make a hypothesis about the change rule of values among grid

points, that is, about their piecewise distribution profile. The finite volume method can satisfactorily overcome the finite element method's weakness of slow calculation, and solve the problem of complex region processing. Thus, we adopted the finite volume method to establish the kinematic model for the landslide flow process.

The core of the finite volume method is domain discretization. The finite volume method uses discrete points as a substitute for continuous space. The physical meaning of the discrete equation is the conservation of the dependent variable in a finite control volume. Establishment of the conservation equation is based on the continuous movement model, that is, the continuity hypothesis about landslide substances. We divided the landslide mass into a series of units and made the hypothesis that each unit has consistent kinematic parameters (speed at a depth, density, etc.) and physical parameters (Fig.1). We also established an Eulerian coordinate system-based conservation equation with regard to each control volume.

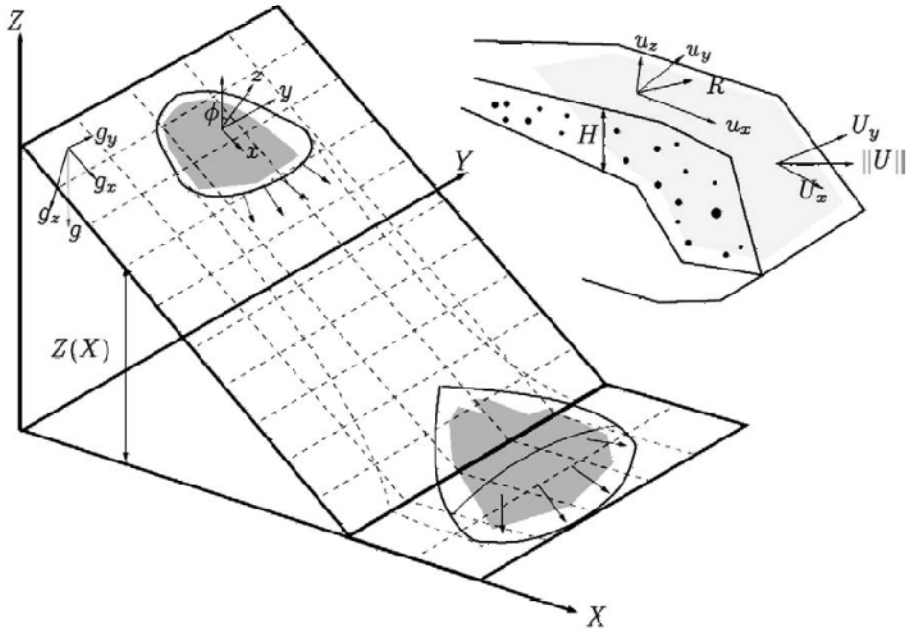

Fig.1 Schematic diagram of finite volume discretization (Christen et al., 2010a).

2.2 Control equation

The computational domain is defined as directions x and y, and the topographic elevation is given the coordinate $z(x,y)$. $H(x,y,t)$ is assumed as the change relationship of landslide thickness with time; $U_x(x,y,t)$ and $U_y(x,y,t)$ respectively represent the mean movement speeds along directions x and y at moment t; $n_x = U_x \Big/ \sqrt{U_x^2 + U_y^2}$ and $n_y = U_y \Big/ \sqrt{U_x^2 + U_y^2}$ represent the cosinoidal and sinusoidal flow vectors of the landslide on the plane x-y. The mean flow speed of

109 substances is defined as $U = \sqrt{U_x^2 + U_y^2}$.

110 Thus, the mass balance equation becomes:

111 $$\partial_t H + \partial_x (HU_x) + \partial_y (HU_y) = \dot{Q} \tag{1}$$

112 wherein, $\dot{Q}(x, y, t)$ represents the change rate (entrainment rate) of landslide
113 volume with time.

114 Assuming that $l(x, y, t)$ represents the movement distance of the landslide with
115 time, we can obtain:

116 $$\dot{Q} = \begin{cases} 0 & if \quad h_i = 0 \\ \dfrac{\rho_i}{\rho_a} h_i \dfrac{U}{l} & if \quad k_i l \geq h_i \\ \dfrac{\rho_i}{\rho_a} k_i U & if \quad k_i l < h_i \end{cases} \tag{2}$$

117 wherein, h_i represents the thickness of the i th layer of the landslide in the
118 movement process; ρ_i represents the density of the i th layer of the landslide in the
119 movement process; ρ_a represents the density of the landslide; the dimensionless
120 parameter k_i represents the entrainment rate.

121 The momentum balance equation is:

122 $$\partial_t \left(HU_x\right) + \partial_x (HU_x^2 + \frac{g_z k_{a/p} H^2}{2}) + \partial_y (HU_x U_y) = S_{gy} - S_f(R)\left[n_x\right] \tag{3}$$

123 $$\partial_t \left(HU_y\right) + \partial_y (HU_y^2 + \frac{g_z k_{a/p} H^2}{2}) + \partial_x (HU_x U_y) = S_{gx} - S_f(R)\left[n_y\right] \tag{4}$$

124 wherein, $S_{gx} = g_x H$ and $S_{gy} = g_y H$ represent the dynamic components of the
125 acceleration of gravity in directions x and y ; $g = (g_x \quad g_y \quad g_z)$ represents the
126 vector of the acceleration of gravity; $k_{a/p}$ represents the pressure coefficient of soil;
127 ρ_a represents the density of the landslide; the dimensionless parameter k_i
128 represents the entrainment rate; $S_f(R)$ represents the frictional resistance.

129 The kinetic energy balance equation is:

130 $$\partial_t (HR) + \partial_x (HRU_x) + \partial_y (HRU_y) = \dot{P} - \dot{D} \tag{5}$$

wherein, $R(x,y,t)$ represents the random mean kinetic energy of the landslide; $\dot{P}(x,y,t)$ and $\dot{D}(x,y,t)$ represent the random increased kinetic energy and decreased kinetic energy of the landslide.

2.3 Constitutive relationship

The improved Voellmy rheological model is applied in the computational simulation of the landslide. See the computational formula below:

$$S_f = \frac{u_i}{\|U\|}\left(h\mu g_z + R_t U^2 + R_\zeta U^2\right) \tag{6}$$

$$R_t = \mu h \frac{U^T K U}{U^2}, R_\zeta = \frac{g}{\zeta} \tag{7}$$

wherein, $u_i/\|U\|$ represents the unit vector in the movement direction of the landslide; μ represents the Coulomb friction coefficient, and is related to $R(x,y,t)$, the random mean kinetic energy of the landslide; R_t represents the gravity-related frictional force coefficient; K represents the substrate surface curvature; ζ represents the viscous friction coefficient of the "turbulent flow".

2.4 HLLE-Heun numerical solution

Synthesizing control equations (1), (3), (4) and (5), we can obtain the simplified form of the nonlinear hyperbola equation:

$$\partial_t V + \nabla \cdot F(V) = G(V) \tag{8}$$

$$V = \begin{pmatrix} H \\ HU_x \\ HU_y \\ HR \end{pmatrix} \qquad G(V) := \begin{pmatrix} \dot{Q} \\ S_{gx} - S_{fx} \\ S_{gy} - S_{fy} \\ \dot{P} - \dot{D} \end{pmatrix}$$

$$F(V) = \begin{pmatrix} HU_x & HU_y \\ HU_x^2 + g_z k_{a/p} \dfrac{H^2}{2} & HU_x U_y \\ HU_x U_y & HU_y^2 + g_z k_{a/p} \dfrac{H^2}{2} \\ HRU_x & HRU_y \end{pmatrix}$$

wherein, $V(x,y,t)$ represents a vector equation consisting of four unknown vector variables; $F(V)$ represents the flux function; $G(V)$ represents the source term. Based on the HLLE equation of the finite volume method and the quadrilateral grid, the node layout can adopt the grid center pattern, and the normal flux along one side of the control volume can be represented by the flux at the center of the side. The

finite volume discretization adopting the control volume as unit is depicted in Fig.1; the Gauss theorem can be followed for the integration of equation (8), wherein C_i represents the unit volume; after converting the volume integral flux function $F(V)$ into the curved surface integral, we can obtain:

$$\int_{C_i} \partial_t V dx + \oint_{\partial C_i} F(V) \cdot n_i d\sigma = \int_{C_i} G(V) dx \tag{9}$$

wherein, n_i represents the outward normal direction vertical to unit C_i at the boundary; through adopting the HLL format for the discretization of surface integral, the following simplified form can be obtained:

$$V_i^{(*)} = V_i^{(n)} + \frac{\Delta t}{A_{C_i}} \Delta F_i^{(HLL)} \left(V^{(n)} \right) \tag{10}$$

$$V_i^{(**)} = V_i^{(*)} + \frac{\Delta t}{A_{C_i}} \Delta F_i^{(HLL)} \left(V^{(*)} \right) \tag{11}$$

$$V_i^{(n+1)} = \frac{1}{2} \left(V_i^{(n)} + V_i^{(**)} \right) \tag{12}$$

wherein, $V_i^{(n)}$ represents the mean value of unit variables at moment $t^{(n)}$; $V^{(n)}$ represents the mean value of the entire grid at moment $t^{(n)}$; $\Delta t := t^{(n-1)} - t^{(n)}$ represents the calculated time step; A_{C_i} represents the area of unit C_i; $\Delta F_i^{(HLL)}$ represents the approximate value of the curved surface integral, as shown below:

$$\Delta F_i^{(HLL)} \left(V^{(n)} \right) := -\sum_{j=1}^{4} F_{ij}^{(HLL)} \left(V^{(n)} \right) n_{ij} \Delta X \tag{13}$$

wherein, n_{ij} represents the outward normal direction of the i th unit at boundary j; the flux calculation term $F_{ij}^{(HLL)} \left(V^{(n)} \right)$ represents the approximate solution mode of the Riemann problem of the i th unit at boundary j; see the computational formula below:

$$F_{ij}^{(HLL)} \left(V^{(n)} \right) = \begin{cases} F \left(V_L^{(n)} \right) & 0 \le S_L \\ \dfrac{S_R F \left(V_L^{(n)} \right) - S_L F \left(V_R^{(n)} \right) + S_R S_L F \left(V_R^{(n)} - V_L^{(n)} \right)}{S_R - S_L} & S_L \le 0 \le S_R \\ F \left(V_R^{(n)} \right) & S_R \le 0 \end{cases} \tag{14}$$

wherein, $V_L^{(n)}$ and $V_R^{(n)}$ respectively represent the approximate values of $V^{(n)}$

on both sides of boundary j of the ith unit; S_L and S_R respectively represent the wave speeds on the left and right sides. Refer to the computational method described by Toro (1992). In addition, the gradient magnitude in the original second-order difference equation can be limited through multiplication with the flux limiter, and the second-order format of the TVD property can be constructed to avoid the occurrence of numerical oscillation. Refer to the specific method described by LeVeque (2002).

In this paper a numerical solver within RAMMS is used, which was specifically designed to provide landslide (avalanche) engineers with a tool that can analyze problems with two-dimensional depth-averaged mass and momentum equations on three-dimensional terrain using both first and second-order finite volume methods (Christen et al., 2010b).

3. Study area and data

3.1 Taziping landslide

The Taziping landslide is located southeast of the Hongse Village, Hongkou Town, Dujiangyan City of Sichuan Province. The site is located at (E103°37′46″, N31°6′29″), 68 km west Chengdu City and 20 km from the Dujiangyan Urban District (Fig. 2). Its geomorphic unit is a middle-mountain tectonic erosional area on the north bank of the Baisha River Valley. The Taziping Landslide is a large-scale colluvial layer landslide triggered by the Wenchuan Earthquake (Fig. 3). It has a gradient of 25°-40° with an average gradient of 32°. The landslide has an apparent round-backed armchair contour with a steep rear edge, which has a gradient of 35°-50° and an elevation of about 1,370 m. The front edge is located on the south side of the mountain road, and has an elevation of about 1,007 m. The landslide has an elevation difference of about 363 m, and a main sliding direction of 124°NE. The landslide mass forms an irregular semi-elliptical shape, and has a length of about 530 m, an average width of 145 m and an area of approximately 7.68×10^4 m^2. The landslide mass is composed of gravelly soil and is covered on by silty clay mingled with gravel. In terms of spatial distribution, the landslide is thick in the middle and thin on the lateral edges, has a thickness of 20-25 m and a volume of approximately 1.16×10^6 m^3. During the earthquake, the landslide mass slid to cover the northern mountain slope of the Hongse Village Miaoba settlement. The landslide has an apparent front edge boundary, and there is also a swelling deformation (Fig. 4).

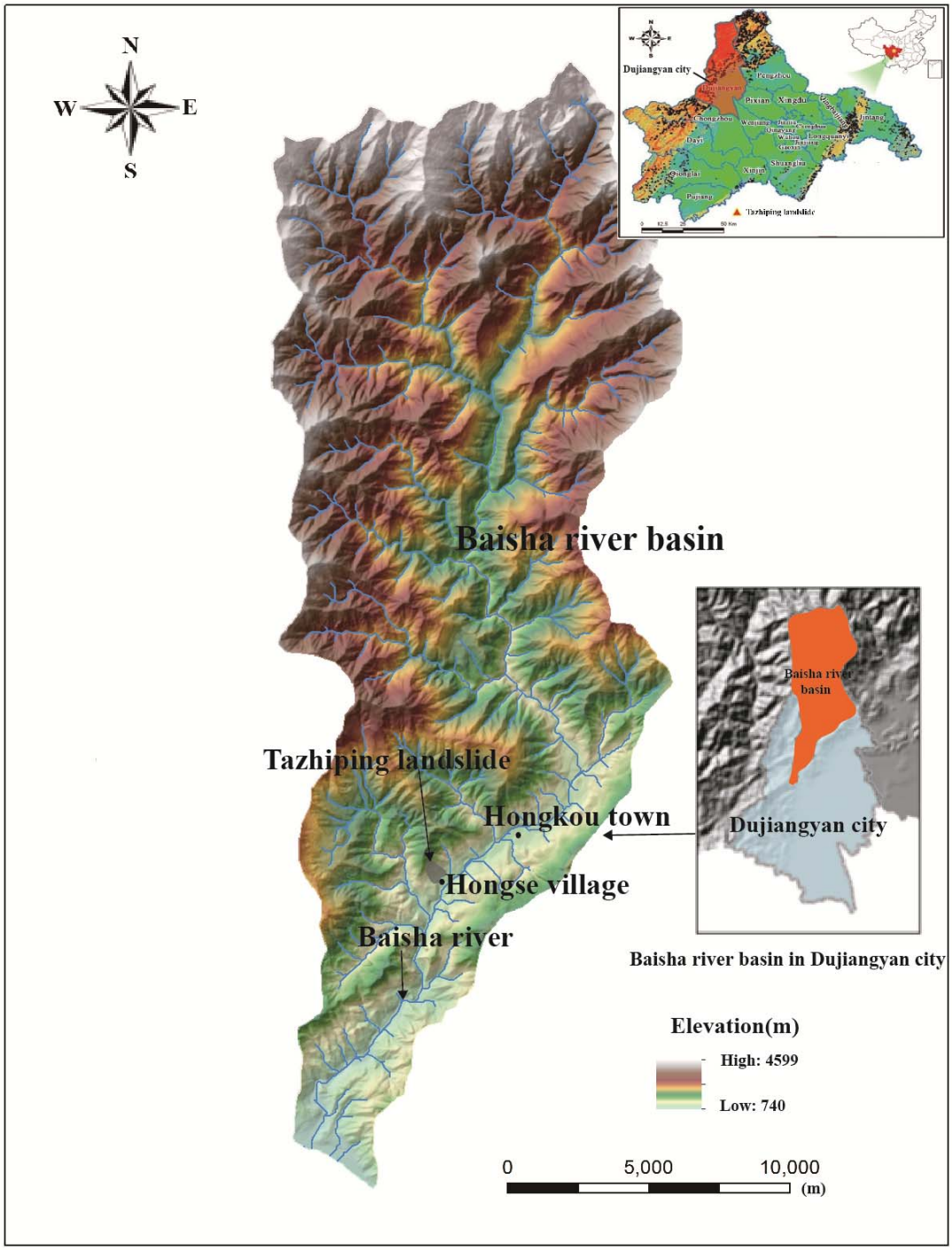

Fig.2 Location of Tazhiping landslide, Baisha river basin, Dujiangyan city (the landslide was triggered by Wenchuan Ms 8.0 earthquake on May 12, 2008)

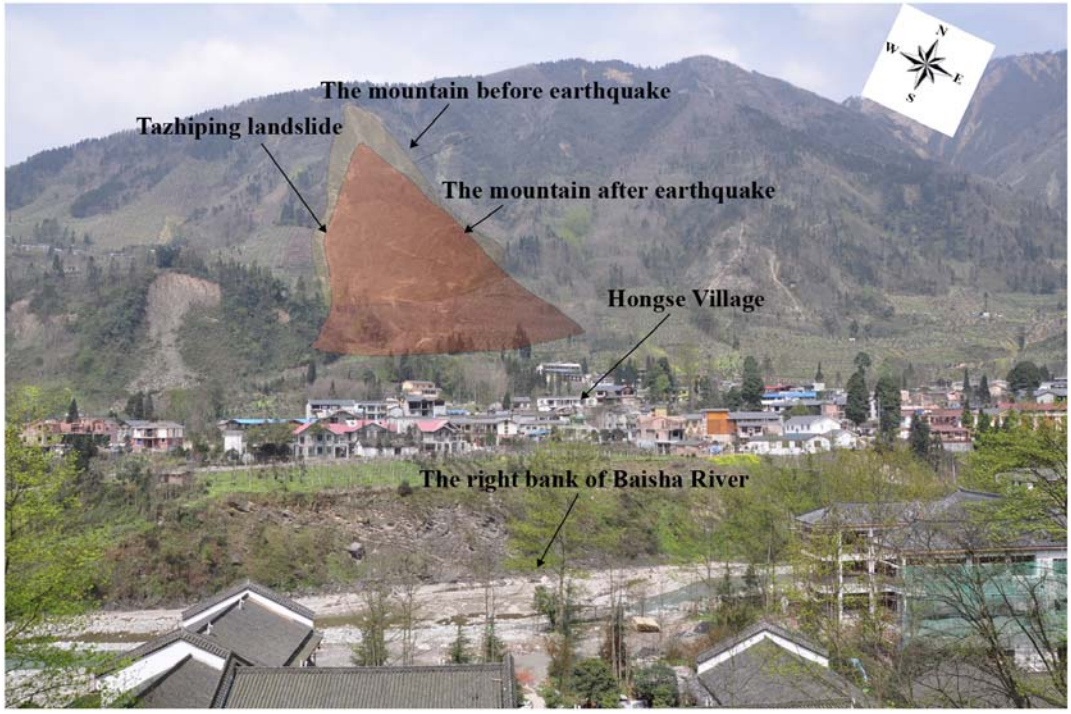

Fig.3 Taziping Landslide

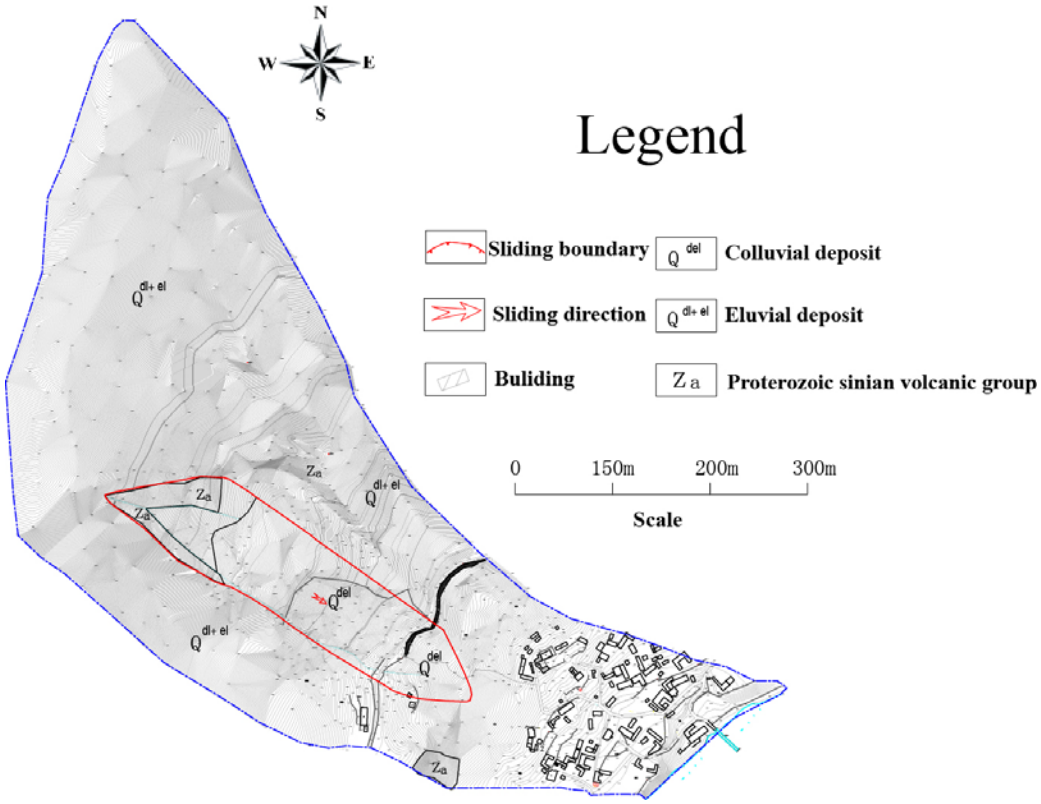

Fig.4 Plane sketch of the Tazhiping landslide

After the Wenchuan Earthquake, the massive colluvial deposits covered the mountain slope. The colluvium is 0.5-5.0 m thick at the top of the slide and is composed of rubble and gravel. The mass consists of a small amount of fine gravel,

which is composed of gray or grayish-green andesite with a clast of 20-150 cm. Field surveys indicate that the rubble in the surface layer has a maximum diameter exceeding 2 m, and that fine gravel is loosely intercalated with the rubble. A small amount of yellowish-brown and gray-brown silty clay mixed with 5-40% of non-uniformly distributed rubble composed the first 5-10 m of the slide. From 10-25 m deep, there is a wide distribution of gravelly soil. The soil is grayish-green or variegated in color, is slightly compact and non-uniform, and has a rock fragment content of about 50%. The parent rock of the rock fragments is andesite, filled with silty clay or silt (Fig.5). Table 1 shows the parameters of the surface gravelly soil of the landslide mass based on the field sampling.

Tab.1 Parameters of surface soil of Taziping Landslide

Internal friction angle (°)		Cohesion (kPa)	Relative compactness	Natural void ratio	Dry density ($kN \cdot m^{-3}$)	Specific gravity ($g \cdot cm^{-3}$)
Peak	Residual					
27.5	23	20.5	53%	0.789	15.357	2.492

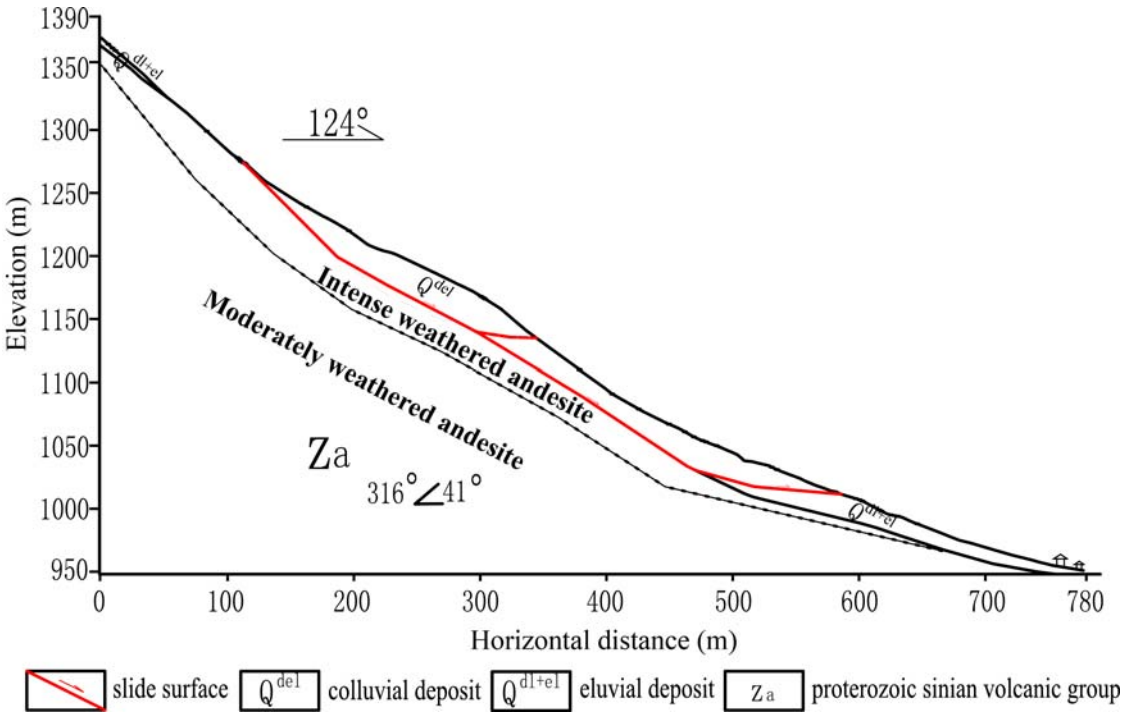

Fig.5 Geological profile of the Taziping Landslide

The landslide is an unconsolidated mass containing relatively large amounts of crushed stones and silty clay (Fig.6). Its loose structure and strong permeability facilitate infiltration of surface water. The Wenchuan earthquake aggravated the deformation of the landslide making deposits more unconsolidated, further reducing the stability of the landslide mass. During persistent rainfall, surface water infiltrates the landslide slope resulting in increased water pressure within the landslide mass and

reduced shear strength on the sliding surface. Thus, rainfall constitutes the primary inducing factor of the upper Taziping landslide. After infiltrating the loose layer, water saturates the slope increasing the dead weight of the sliding mass and reducing the shear strength of soil in the sliding zone. Infiltration into the landslide mass also increases the infiltration pressure of perched water, drives deformation, and poses a great threat to villages located at the front of the landslide. Slide-resistant piles and backfill were place at the toe of the slope in order to reduce the hazards of future slides. The slide-resistant piles have enhanced the overall stability of the slope, however, under heavy rainfall the upper unconsolidated landslide deposits may cut out from the top of the slide-resistant piles.

(a) Material on the landslide surface (b) Material in the shear zone

Fig.6 Photographs showing colluvial deposit cover on the mountain slope

Therefore we simulate possible movement states of the Taziping landslide before and after treatment with slide-resistant piles, comparatively analyzed the kinetic parameters in the movement process, and mapped the 2D division of hazard zones.

3.2 Hazard prediction before treatment

It was assumed that the landslide was damaged before engineering treatment. According to field investigation, the sliding mass had an estimated starting volume of about 600,000m^3 and a mean thickness of 8m. Based on the survey report and field investigation (Hydrologic Engineering and Geological Survey Institute of Hebei Province, 2010), we adopted the survey parameters of Tab.2 for the simulated calculation. These parameters were obtained from laboratory or small-scale experiments and back-analyses of relatively well-documented landslide cases. The unit weigh $\gamma = 20.8kN \cdot m^{-3}$ is from small-scale conventional triaxial test experiments in laboratory. In addition, we selected the coulomb friction coefficient $\mu = 0.45$ and viscous friction coefficient $\zeta = 500m \cdot s^{-2}$ in accordance with back-analyses of well-documented landslide cases (Cepeda et al., 2010; Du et al., 2015). The erosional entrainment rate selected was the minimum value $k_i = 0.0001$ in the RAMMS program.

Tab.2 Model calculation parameters

Unit weight $\gamma(kN \cdot m^{-3})$	**Coulomb friction coefficient** μ	**Viscous friction coefficient** $\zeta(m \cdot s^{-2})$	**Erosional entrainment rate** k_i
20.8	0.45	500	0.0001

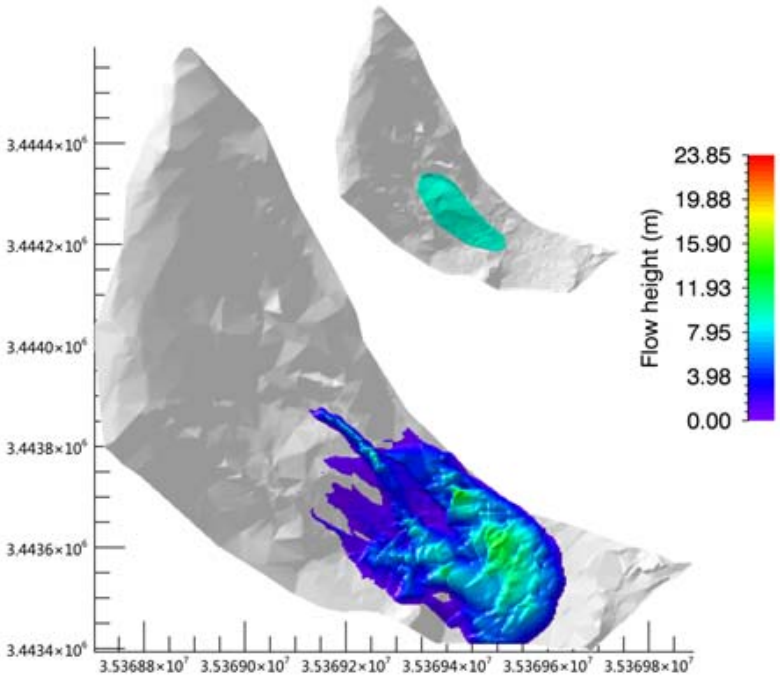

(a) Flow height

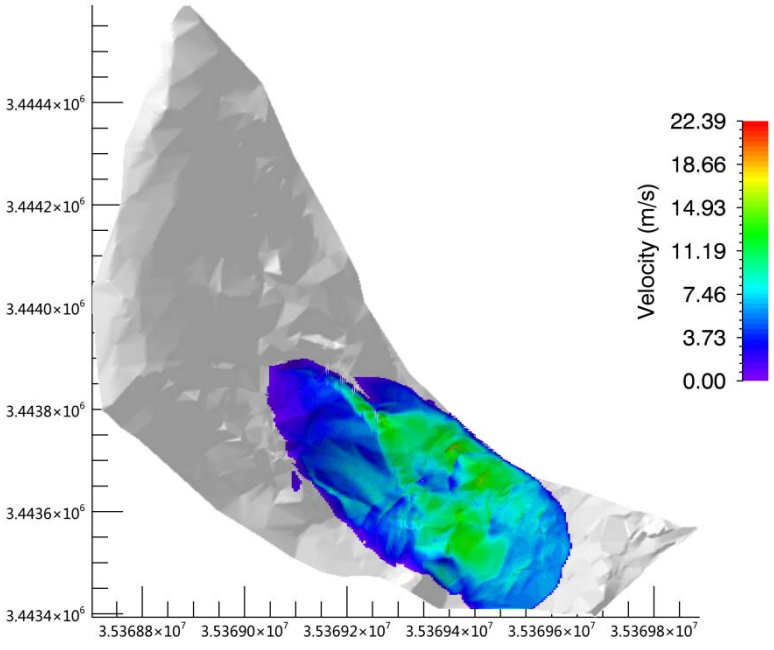

(b) Velocity

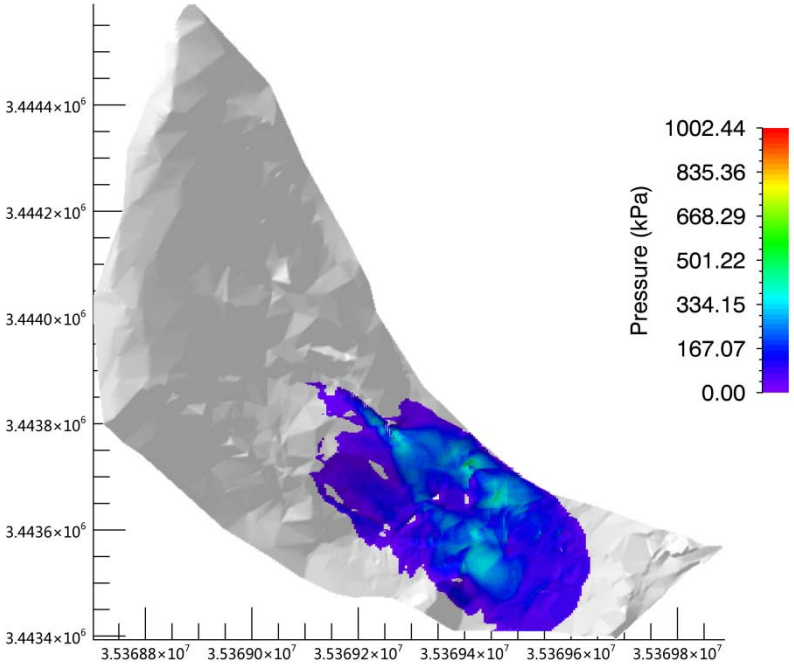

(c) Pressure

Fig. 7 Movement characteristic parameters of the Taziping landslide (before treatment)

See the kinematic characteristic parameters of the landslide deposits in Fig.7. The colored bar shows the maximum values of the kinematic process for a given time step. As shown by the calculation results, deposits accumulated during the landslide movement process had a maximum flow height of 23.85m, located around the surface gully of the middle and upper slope. The middle and lower section of the landslide deposit had a flow height of about 5-10m; the middle and lower movement ~~speed~~ velocity of the landslide ranged from 3m/s and 7m/s; the landslide had a mean pressure of about 500kPa, and the pressure of the middle and lower deposits was about 200kPa. Thus, three-story and lower houses within the deposition range might be buried (The building is 3m high on each floor), and it was further suggested that the design strength of the gable walls of houses on the middle and upper parts of the deposit be increased above 300kPa.

3.3 Hazard prediction after treatment

After fully accounting for the slide-resistant piles and mounds, we introduced the Morgenstern-Price method (Morgenstern et al., 1965) to calculate the stability coefficient of Taziping landslide after treatment. The method was determined with an iterative approach by changing the position of the sliding surface until failure of the dumpsite (Fig.8). The physico-mechanical parameters under a saturated state (Hydrologic Engineering and Geological Survey Institute of Hebei Province, 2010) were adopted to search for the sliding plane of the landslide.

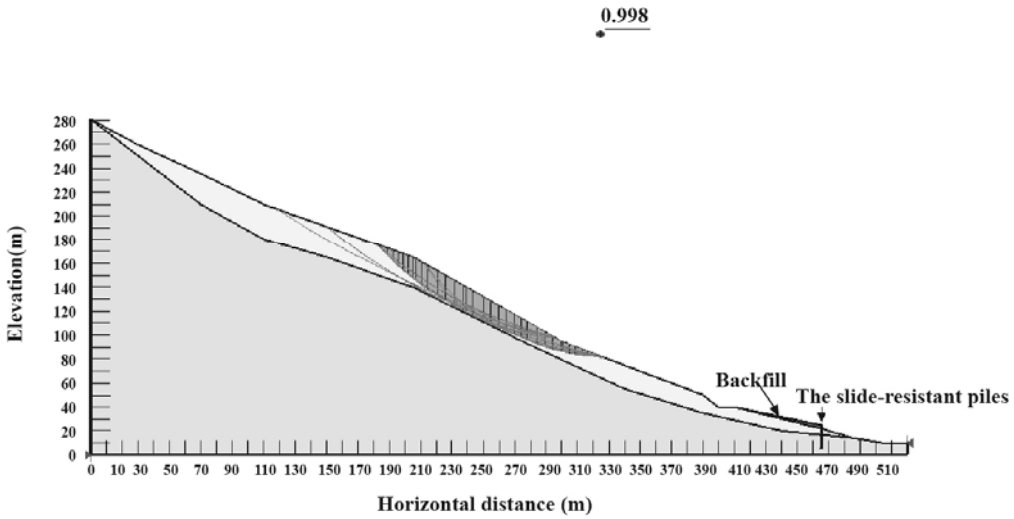

Fig.8 Search for the sliding plane of the Taziping landslide (before treatment)

Based on numerical analysis, the Taziping landslide stability coefficient is 0.998. Under rainfall conditions, the middle area of the Taziping landslide was unstable. Loose deposits in the middle part of the landslide might convert into a high-water landslide and cut out from the top of the slide-resistant piles. In the damaged area, the slope had a rear edge wall elevation of about 1,170m. Its front edge was located on the south side of the mountain road, with an elevation of 1,070-1,072m and a length of 182m. Thus, the scale of the rainfall-damaged is estimated to be about 250,000m^3, with a mean thickness of about 6m. The parameters in Tab.2 were again adopted for the simulated calculation.

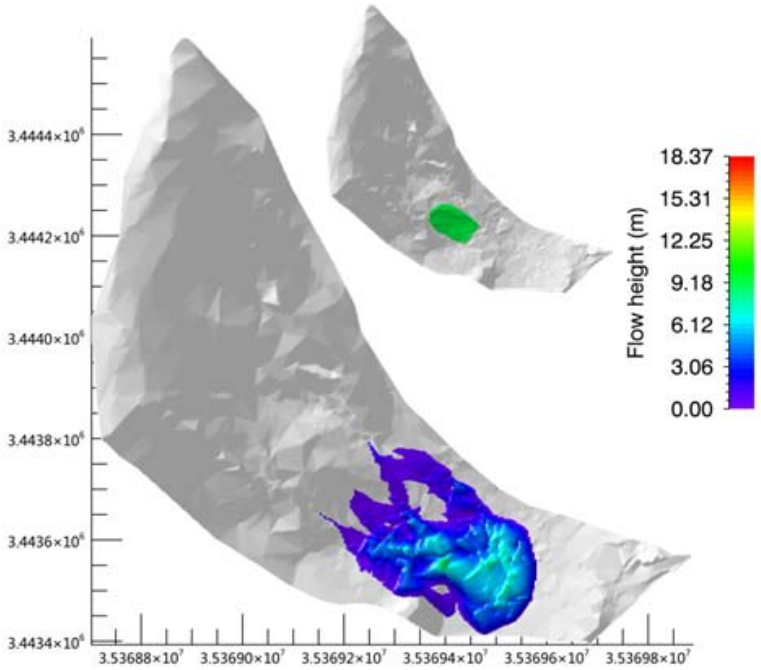

(a) Flow height

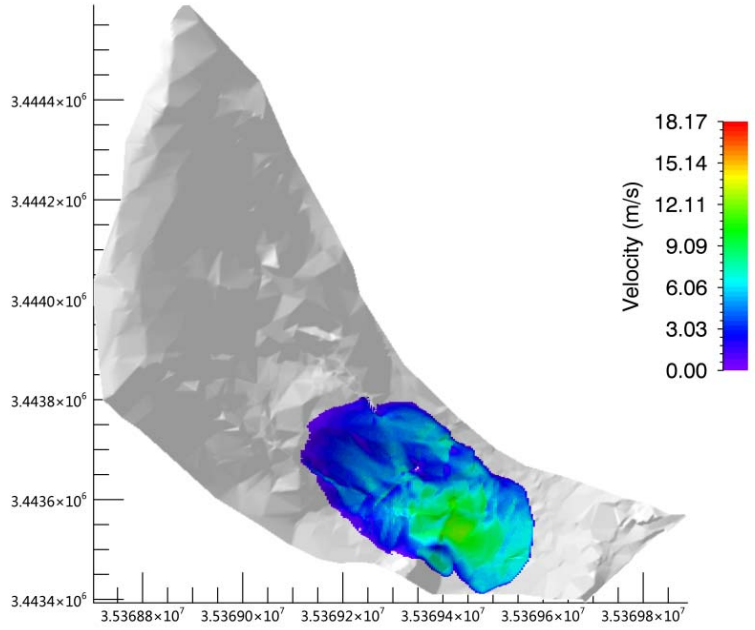

(b) Velocity

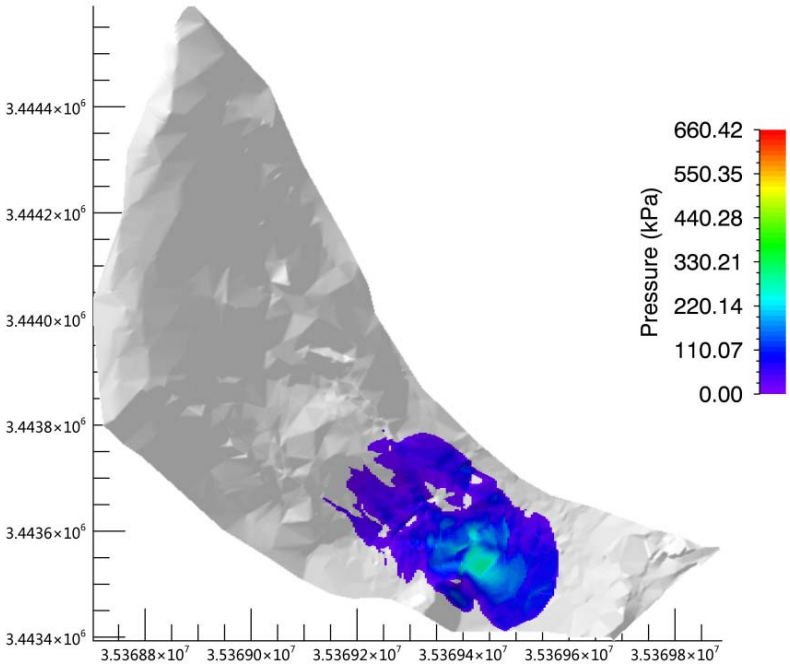

(c) Pressure

Fig. 9 Movement characteristic parameters of the Taziping landslide (after treatment)

Provided in Fig.9 are the kinematic characteristics of the landslide deposit. The colored bar shows the maximum values of the kinematic process for a given time step. Deposits accumulated during the landslide movement process had a maximum flow height of 18.37m, located around the surface gully of the middle and upper slope. The middle and lower portions of the landslide deposit had a flow height of approximately 3-5m. The middle and lower movement velocity of the landslide deposits ranged

between 3m/s and 5m/s. The landslide had a mean pressure of about 330kPa, and the pressure of the middle and lower deposits was about 100kPa. Thus, it could be held that two-story and lower houses within the deposition range might be buried. It was further suggested that the design strength of the gable walls of houses on the middle and upper parts of the deposits be increased above 150kPa.

After treatment, the accumulation flow height and pressure of the deposits were reduced by about 1/2, and the kinematic speed is reduced by about 1/3. However, the Miaoba residential area of Red Village was still partially at hazard.

4 Results

Landslides reflect landscape instability that evolves over meteorological and geological timescales, and they also pose threats to people, property, and the environment. The severity of these threats depends largely on landslide speed and travel distance. There may be examples where entire houses on a landslide mass are moved but not destroyed because of stable base plates. In any case, velocity plays a more important role regarding kinetic energy acting on an obstacle. However, the Miaoba residential area of Red Village is located at the frontal part of Tazhiping lanslide. During landslide movement, the spatial scale indexes of a landslide mass include area, volume, and thickness. The maximum thickness of the landslide is one of the direct factors influencing the building's deformation failure status. A large landslide displacement may lead to burial, collapse, or deformation failure of the building, and thus influence its safety and stability. Thus, landslide thickness constitutes an important index for assessing the hazards of a landslide disaster, and for influencing the consequences faced by disaster-affected bodies (Fell et al., 2008; DZ/T, 0286-2015). Provided in Tab.3 is a landslide thickness-based division of the predicted hazard zones of Taziping landslide, in which the thickness of the landslide mass correlates with the ability of a building to withstand a landslide disaster (Hungr et al., 1984; Petrazzuoli et al., 2004; Glade 2006; GB, 50010–2010; Hu et al., 2012; Zeng et al., 2015). After treatment with slide-resistant piles, the hazard of a future slide was reduced by about 1/3 overall and by 2/3 in high-hazard zones.

Tab.3 Division table of the predicted hazards of Taziping landslide (unit: m^2)

Hazard zone level	Assessment index	Building damage probability	Area before treatment	Area after treatment	Increased/decreased area	Building damage characteristics
Low-hazard zone (l)	h≤0.5m	20%	44，600	38，748	-5,852	One-story houses may be damaged; houses on the

						landslide mass are partially damaged.
Relatively low-hazard zone (Ⅱ)	0.5 m < h≤1m	50~20%	24，900	26，400	+1,500	One-story houses have a very high probability of being damaged; one-story houses on the landslide mass are completely damaged.
Moderate-hazard zone (Ⅲ)	1m < h≤3m	80~50%	21，980	15，856	-6,124	One-story to three-story houses have a very high probability of being damaged; houses less than three stories on the landslide mass are completely damaged.
Relatively high-hazard zone (Ⅳ)	3m < h≤5m	100~80%	30，820	19，636	-11,184	One-story houses may be buried, and two-story to six-story houses have a very high probability of being damaged; houses on the landslide mass are completely

						damaged. Two-story and lower houses may be buried, and three-story and higher houses have a very high probability of being damaged; houses on the landslide mass are completely damaged.
High-hazard zone (Ⅴ)	*h*≥5m	100%	47，240	13，052	-34,188	
Total area:	—	—	169，540	113，700	-54,340	—

The hazard zones of Taziping landslide was given by 2D divisions before and after engineering treatment (Fig. 10). The size of the hazard zones changed after engineering treatment, particularly in the high-hazard zones. Before treatment with slide-resistant piles, the landslide posed a great hazard to eight houses on the left side of the upper Miaoba residential area, with a high-hazard zone associated with landslide mass height over 5m and a red zone. After treatment, the number of effected houses was reduced to four. We defined outside the colored area as no-hazard.

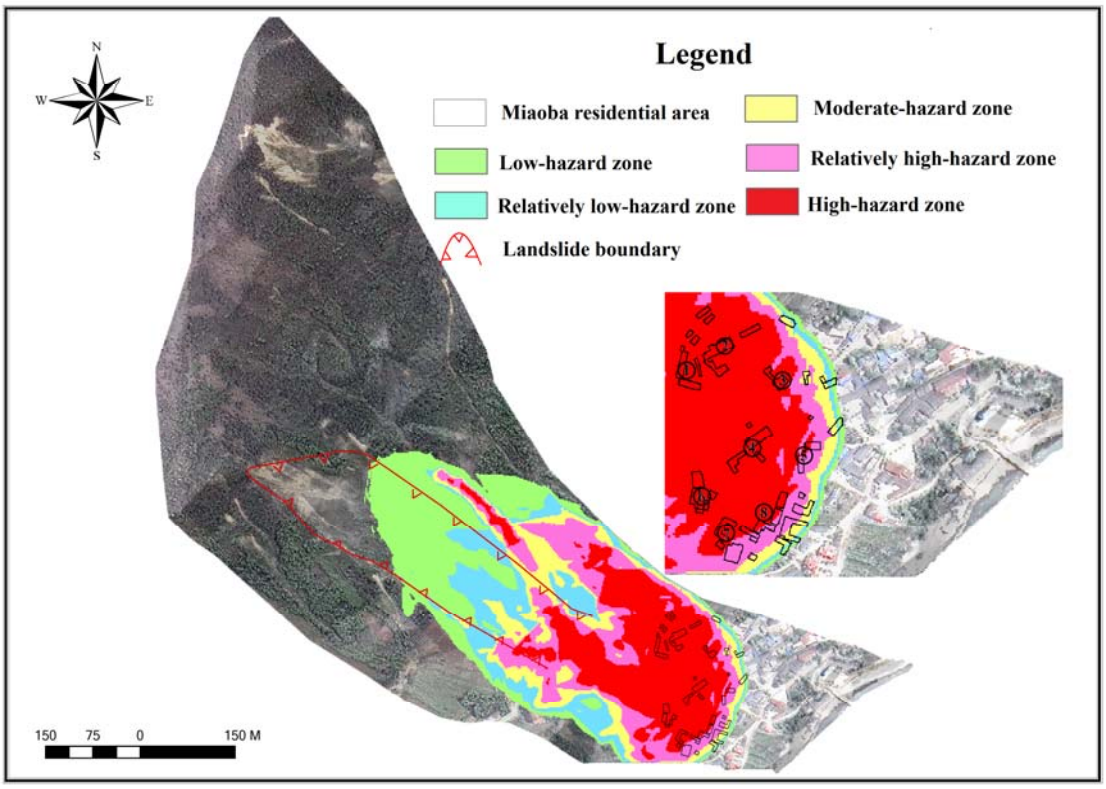

(a) Before treatment

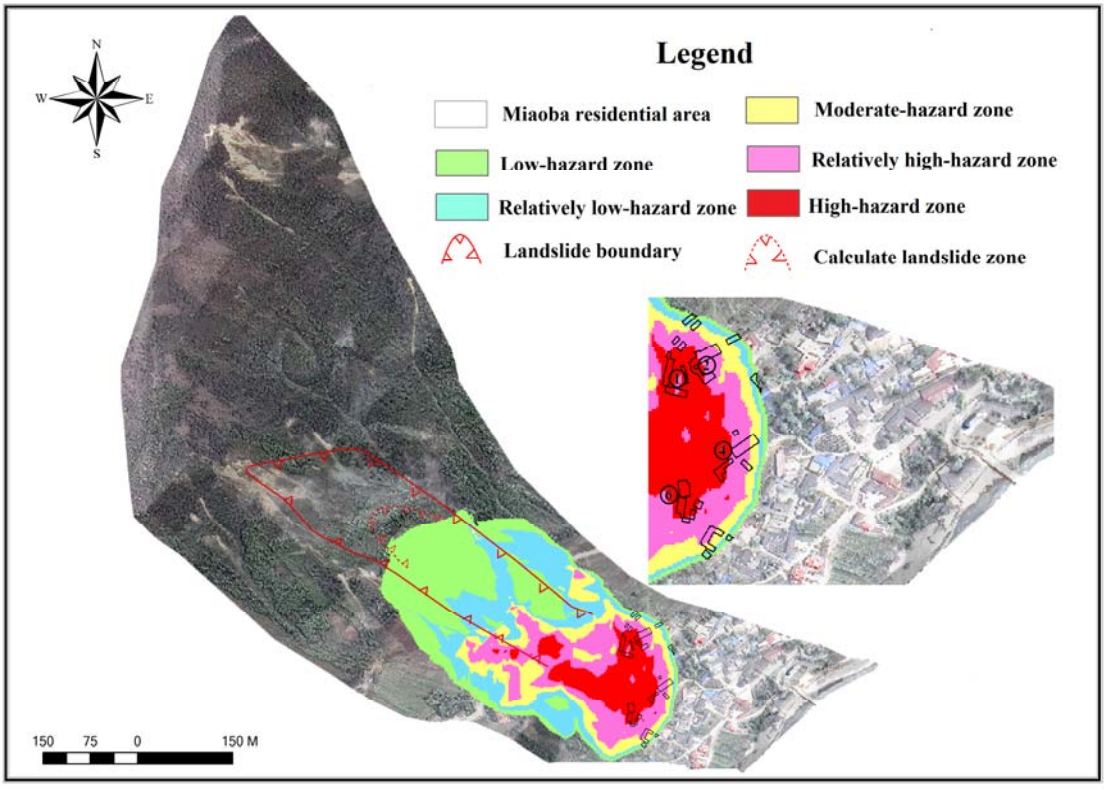

(b) After treatment

Fig. 10 2D division comparison of the hazards of the Taziping landslide

5 Conclusions and Discussion

The hazard assessment of landslides using numerical models is becoming more and more popular as new models are developed and become available for both scientific research and practical applications. There is some confusion about the mass movement process that is discussed by the rheological model presented in this contribution.

Landslides move downslope in many different ways (Varnes, 1978). In addition, landslides can evolve into rapidly travelling flows, which exhibit characteristics of debris flows on unchannelized or only weakly channelized hillslopes. The geomorphic heterogeneity of rapid shallow landslides, such as hillslope debris flows, is larger than observed in channelized debris flows; however many of these flows can be successfully modelled using the Voellmy-fluid friction (Christen et al., 2012). Results presented in this paper support the conclusion that Voellmy-fluid rheological model can be used to simulate flow-type landslides.

The selection of model parameters remains one of the fundamental challenges for numerical calculations of natural hazards. At present, there are numerous empirical parameters obtained from 30-years of monitoring data. Such as in RAMMS, we can automatically generate the friction coefficient of an avalanche for our calculation domain based on topographic data analysis, forest information and global parameters (WSL, 2013). The friction parameters for debris flows can found in some literature (Fannin et al., 2001; Iovine et al., 2003; Hürlimann et al., 2008; Scheidl et al., 2010; Huang et al., 2015). However, there is little research regarding friction parameters of flow-type landslide. Therefore, we tested different coulomb friction coefficient μ values ranging between $0.1 \le \mu \le 0.6$ and viscous friction coefficient ζ values ranging between $100 \le \mu \le 1000 m \cdot s^{-2}$. Finally, we selected the coulomb friction coefficient $\mu = 0.45$ and viscous friction coefficient $\zeta = 500 m \cdot s^{-2}$ in accordance with back-analyses of well-documented landslides (Cepeda et al., 2010; Du et al., 2015). Simulation results are consistent with field observations of topography and sliding path.

Based on the finite volume method and the RAMMS program, simulation results of Taziping landslide were consistent with the sliding path predicted by the field investigation. This correlation indicates that numerical simulation is an effective method for studying the movement processes of flow-type landslides. The accumulation flow height and pressure of landslide deposits were reduced by about 1/2, and the kinematic speed was reduced by about 1/3 after treatment. However, the Miaoba residential area of Red Village is still partially at hazard. Considering that two-story and lower houses within the deposition range might be buried, it was further suggested that the design strength of the gable walls of houses on the middle and upper parts of the deposit be increased above 150kPa.

By utilizing a GIS platform in combination with landslide hazard assessment indexes, we mapped the 2D division of the Taziping landslide hazard zones before

and after engineering treatment. The results indicated that overall hazard zones contracted after engineering treatment and, the area of high-hazard zones was reduced by about 2/3. After engineering treatment, the number of at hazard houses on the left side of the upper Miaoba residential area, was reduced from eight to four. It was thus clear that some zones are still at high hazard despite engineering treatment. Therefore, it was proposed that houses located in high-hazard zones be relocated or reinforced for protection.

Acknowledgments

The authors sincerely acknowledge the CAS Pioneer Hundred 432 Talents Program for the completion of this research. This work was supported by National Natural Science Foundation of China (Grant No. 41301009 41301592) and the Hundred Young Talents Program of IMHE (SDSQB-2016-01), the International Cooperation Program of the Ministry of Science and Technology of China (Grant No.2013DFA21720). The authors express their deepest gratitude to those aids and assistances. The authors also extend their gratitude to editor and two anonymous reviewers for their helpful suggestions and insightful comments, which have contributed greatly in improving the quality of the manuscript.

Reference

Bartelt, P., Bühler, Y., Buser, O., Christen, M., and Meier, L.: Modeling massdependent flow regime transitions to predict the stopping and depositional behavior of snow avalanches, J. Geophys. Res., 117, F01015, doi:10.1029/2010JF001957, 2012 .

Costa, J.E.: Physical geomorphology of debris flows. Developments and Applications of Geomorphology, Springer Press., 268-317, 1984.

Christen, M., Kowalski, J., and Bartelt, P.: RAMMS: Numerical simulation of dense snow avalanches in three-dimensional terrain, Cold Regions Science and Technology., 63, 1–14, 2010.

Christen, M., Bartelt, P., and Kowalski, J.: Back calculation of the In den Arelen avalanche with RAMMS: interpretation of model results, Annals of Glaciology., 51, 161–168, 2010.

Christen, M., Bühler, Y., Bartelt, P., Leine, R., Glover, J., Schweizer, A., Graf, C., McArdell, B., Gerber, W., Deubelbeiss, Y., Feistl, T., and Volkwein, A.: Integral hazard management using a unified software environment: numerical simulation tool “RAMMS” for gravitational natural hazards, In: Koboltschnig, G., Hübl, J., Braun, J. (eds.) Proceedings of 12th Congress INTERPRAE., 1, 77–86, 2012.

Chen, J.C., and Chuang, M.R.: Discharge of landslide-induced debris flows: case studies of Typhoon Morakot in southern Taiwan, Nat. Hazards Earth Syst. Sci., 14, 1719-1730, 2014.

Cepeda, J., Chávez, J.A., and Martínez, C.C.: Procedure for the selection of runout model parameters from landslide back-analyses：application to the Metropolitan Area of San

Salvador, El Salvador, Landslides., 7, 105–116, 2010.
Du, J., Yin, K.L., and Wang, J.J.: Simulation of three-dimensional movement of landslide-debris flow based on finite volume method, Chinese Journal of Rock Mechanics and Engineering., 34: 480–488, 2015 (in Chinese).
Evans, S.G., Tutubalina, O.V., Drobyshev, V.N., Chernomorets, S.S., McDougall, S., Petrakov, D.A., and Hungr, O.: Catastrophic detachment and high-velocity long-runout flow of Kolka Glacier, Caucasus Mountains, Russia in 2002, Geomorphology., 105, 314–321, 2009.
Fannin, R.J., and Wise, M.P.: An empirical-statistical model for debris flow travel distance, Canadian Geotechnical Journal., 38, 982–994, 2001.
Finlay, P.J., Mostyn, G.R., and Fell, R.: Landslide risk assessment: prediction of travel distance, Canadian Geotechnical Journal., 36, 556–562, 1999.
Fell, R., Corominas, J., Bonnard, C., Cascini, L., Leroi, E., and Savage, W. Z.: Guidelines for landslide susceptibility, hazard and risk zoning for land use planning, Engineering Geology., 102, 85–98, 2008.
Fannin, R., and Wise, M.: An empirical-statistical model for debris flow travel distance, Can Geotech J ., 38, 982–994, 2001.
Glade, T.: Linking debris-flow hazard assessments with geomorphology. Geomorphology., 66(1): 189-213, 2005.
Glade, T., Anderson, M. G., Crozier, M.J.: Landslide hazard and risk. Wiley., 75-138, 2006.
GB 50010–2010.: Code for design concrete structures, Beijing: Chinese Architectural Industry., 34–80, 2010 (in Chinese).
Hebei Province Institute of Hydrogeological and Engineering.: Geological investigation engineering supplemental survey report of Hongse Village Taziping landslide in Hongkou Town of Dujiangyan City, Sichuan Province., 2010 (in Chinese).
Hungr, O.: A Model for the runout analysis of rapid flow slides, debris flows and avalanches, Can Geotech J ., 32, 610–623, 1995.
Hungr, O., Evans, S.G., Bovis, M,J., and Hutchinson, J,N.: A review of the classification of landslides of the flow type, Environ Eng Geosci., 7, 221–238, 2001.
Hungr, O., Morgan G.C., and Kellerhals, R.: Quantitative analysis of debris torrent hazards for design of remedial measures, Can Geotech J., 21, 663–677, 1984.
Hu, K.H., Cui, P., and Zhang, J.Q., Characteristics of damage to buildings by debris flows on 7 August 2010 in Zhouqu, Western China, Nat Hazards Earth Syst Sci., 12, 2209–2217, 2012.
Hürlimann, M., Rickenmann, D., Medina, V., and Bateman, A.: Evaluation of approaches to calculate debris-flow parameters for hazard assessment, Eng Geol., 102, 152–163, 2008.
Huang, Y., Cheng, H., Dai, Z., Xu, Q., Liu, F., Sawada, K., Moriguchi, S., and Yashima, A.: SPH-based numerical simulation of catastrophic debris flows after the 2008 Wenchuan earthquake, Bull Eng Geol Environ., 74, 1137–1151, 2015.
Iverson, R. M., Reid, M. E., and LaHusen, R. G.: Debris-flow mobilization from landslides, Annu. Rev. Earth Planet Sc., 25, 85– 138, 1997.
Iverson, R.M., and Vallance, J.W.: New views of granular mass flows, Geology., 29, 1115–1118, 2001.
Iovine, G., Gregorio, S,D., and Lupiano, V.: Debris-flow susceptibility assessment through cellular automata modeling: an example from 15–16 December 1999 disaster at Cervinara and San Martino Valle Caudina (Campania, southern Italy), Nat Hazards Earth Syst Sci., 3, 457–468,

2003.
Jackson, L.E., Kostashuk, R.A., and MacDonald, G.M.: Identification of debris flow hazard on alluvial fans in the Canadian Rocky mountains, Geological Society of America., 7, 155–124, 1987.
LeVeque, R.: Finite Volume Methods for Hyperbolic Problems, Cambridge Texts in Applied Mathematics Cambridge University Press., 2002.
Michael-Leiba, M., Baynes, F., Scott, G., and Granger, K.: Regional landsliderisk to the Cairns community, NatHazards., 30, 233–249, 2003.
Morgenstern, N.R., and Price, V.E.: The analysis of the stability of general slip surfaces, Geotechnique., 15, 79–93, 1965.
Portilla, M., Chevalier, G., and Hürlimann, M.: Description and analysis of the debris flows occurred during 2008 in the Eastern Pyrenees, Nat. Hazards Earth Syst. Sci., 10, 1635–1645, 2010.
Petrazzuoli, S,M., and Zuccaro, G.: Structural resistance of reinforced concrete buildings under pyroclastic flows: a study of the Vesuvian area, J Volcanol Geoth Res., 133, 353–367, 2004.
Sassa, K., Nagai, S., Solidum, R., Yamazaki, Y., and Ohta, H.: An integrated model simulating the initiation and motion of earthquake and rain induced rapid landslides and its application to the 2006 Leyte landslide, Landslides., 7, 219–236, 2010.
Scott, K.M., and Vallance, J.W.: History of Landslides and Debris Flows at Mount Rainier: Water Fact Sheet, USGS Open-File Report., 93–111, 1993.
Shi,G.H.: Discontinuous deformation analysis - a new numerical model for the statics and dynamics of block system, Berkeley: University of California., 1988.
DZ/T 0286-2015.: Specification of risk assessment for geological hazard, Ministry of Land and Resources of the People's Republic of China., 2015 (in Chinese).
Scheidl, C., and Rickenmann, D.: Empirical prediction of debris-flow mobility and deposition on fans, Earth Surf Proc Land., 35, 157–173, 2010.
Toro, E.F.: Riemann problems and the waf method for solving the two dimensional shallow water equations. Philos. Trans. R. Soc. London., Ser. A 338, 43–68, 1992.
Varnes, D.J., : Slope movement types and processes. In: Schuster RL, Krizek RJ (eds) Landslides: analysis and control. Transportation Research Board, National Research Council, Washington, DC, USA., 11–33 , 1978.
Wang, L., Li, B., Gao, Y., and Zhu, S.: Run-out prediction of large thick-bedded unstable rock: A case study of Daxiang unstable rock in Yangjiao town, Wulong county, Chongqing, Earth Science Frontiers., 23, 251–259, 2016 (in Chinese).
WSL.: RAMMS: A numerical model for snow avalanches in research and practice, User manual v1.5 avalanche, WSL Institute for snow and avalanche research SLF, Swiss., 2013.
Zeng, C., Cui, P., Su, Z.M., Lei, Y., Chen, R.: Failure modes of reinforced concrete columns of buildings under debris flow impact, Landslides., 12, 561-571, 2015.